



HAL
open science

Active resonance damping and harmonics compensation in distributed generation based islanded microgrids

Abdelhakim Saim, Azeddine Houari, Mourad Aït-Ahmed, Mohamed Machmoum, Josep M. Guerrero

► To cite this version:

Abdelhakim Saim, Azeddine Houari, Mourad Aït-Ahmed, Mohamed Machmoum, Josep M. Guerrero. Active resonance damping and harmonics compensation in distributed generation based islanded microgrids. *Electric Power Systems Research*, 2021, 191, pp.106900. 10.1016/j.epsr.2020.106900 . hal-03494060

HAL Id: hal-03494060

<https://hal.science/hal-03494060>

Submitted on 7 Nov 2022

HAL is a multi-disciplinary open access archive for the deposit and dissemination of scientific research documents, whether they are published or not. The documents may come from teaching and research institutions in France or abroad, or from public or private research centers.

L'archive ouverte pluridisciplinaire **HAL**, est destinée au dépôt et à la diffusion de documents scientifiques de niveau recherche, publiés ou non, émanant des établissements d'enseignement et de recherche français ou étrangers, des laboratoires publics ou privés.



Distributed under a Creative Commons Attribution - NonCommercial 4.0 International License

Active Resonance Damping and Harmonics Compensation in Distributed Generation based Islanded Microgrids

Abdelhakim Saim^{a, b*}, Azeddine Houari^a, Mourad Ait-Ahmed^a, Mohamed
Machmoum^a, Josep. M Guerrero^c

^a IREENA Laboratory, University of Nantes, France.

^b LSEI Laboratory, University of Sciences and Technology Houari Boumediene, Algeria.

^c Center for Research on Microgrids (CROM), Aalborg University, Denmark.

* Corresponding author e-mail: abdelhakim.saim@univ-nantes.fr / asaim@usthb.dz

1 existing electrical facilities [3]. These small-scale grid configurations connect multiple
2 DG units, storages and loads to form single controllable entities [4]. Those entities can
3 operate either in grid-connected or in islanded mode in order to provide end-users with
4 reliable service even during contingencies [5].

5 In islanded mode of operation, these systems may present some weaknesses to handle
6 disturbances due to their reduced rotational inertia and short-circuit power capacity [6].
7 This is mainly due to the increasing integration of power electronics based DG units and
8 loads appliances with high share of intermittent energy resources [7]. More specifically,
9 these systems can face multiple disturbances either at low or high frequency ranges [8].
10 Low frequency disturbances can be introduced by load changes and sources
11 intermittency [9]. Besides, high frequency disturbances can appear as the circuit
12 configuration of MGs is prone to resonances phenomena [10]. These phenomena are due
13 to the use of high order passive filters with inherent resonance characteristics such as LC
14 and LCL filters [11]. These resonances result in harmonics amplification, which
15 increases current and voltage distortion [12]. Moreover, interactions could happen
16 among the interconnected DG units and the background system, which can result in
17 multiple resonances [13]. The risk of resonances is augmented by the increasing usage of
18 nonlinear and unbalanced electronic load appliances [14]. The characteristic frequencies
19 of these resonances may vary and additional resonances may appear once more DG units
20 and loads are connected to the MG [15]. These resonances can propagate and affect the
21 whole MG as DG units and loads are coupled through small line impedances [16]. This
22 situation represents an important matter in MGs since it affects power quality, increases
23 losses, damages electronics, and can even lead to system instability [17].

24 The damping of such resonances is still a challenging task that requires the
25 development of advanced analysis and damping methods. Several researches

1 contributing to resonance analysis and damping in MGs are proposed in the literature
2 [18]. These methods use either passive or active damping approaches. Passive damping
3 approaches are based on the filter circuit reconfiguration through the addition of energy
4 dissipative elements [19], [20]. Although the passive damping shows robust damping
5 performances, the use of active damping is preferred since it allies efficiency and
6 flexibility, which is of importance to achieve scalable MG functionality. The active
7 damping uses either filter-based or feedback-based control methods. The feedback based
8 methods consider the use of complementary control loops in order to obtain a wider
9 damping region [21]. These methods feedback either the capacitor current through a high
10 pass filter, or similarly the capacitor voltage through a low pass filter to achieve the
11 desired damping performances [22]. Similarly, the filter inductor current can be used for
12 damping purpose [23]. Although these methods achieve satisfactory damping
13 performances, the control complexity is increased and additional measurements are
14 required [24]. This results in extra costs and increases the computational effort, which
15 limits their practical implementation.

16 Besides, the filter based methods incorporate additional filters to the control system
17 with the aim to mitigate the undesired dynamic [25]. These methods commonly use lead-
18 lag compensators, high pass filters, or notch filters achieving satisfactory damping
19 performances [26]. However, these methods remain sensitive to parameters uncertainties
20 and their efficiency depends on the accuracy of the resonance frequency estimate. Self-
21 commissioning filters with complex structures have been proposed in the literature to
22 achieve adaptive damping solutions [27]. These methods can affect the control dynamic,
23 which limits their applicability in MGs wherein hierarchical strategies with multi-levels
24 multi-loops controllers are usually adopted. In order to achieve resonances damping and
25 preserve the system dynamic, the introduction of an external active damping control loop

1 has been proposed in [28]. Although this method achieves suitable damping
2 performances while preserving the system dynamic, it involves a complex design
3 procedure with multi-parameters setting.

4 In this paper, a hierarchical control strategy with harmonics compensation and active
5 resonance damping is proposed to control islanded MGs operation and dampen out the
6 undesired resonance amplifications. The proposed method uses a washout filter with
7 inherent stability characteristics to reconstruct and compensate for resonance harmonics.
8 It uses an external control level that superposes the resulting harmonics-compensating
9 signal directly on the control signal, which preserves the dynamic of the inner control
10 levels. This method offers simplicity of design and implementation with the ability to
11 achieve resonance damping even for uncertain MG configurations. More specifically,
12 and considering the context of islanded MGs, this method presents the following
13 advantages:

- 14 • Straightforward to design and implement without the need for additional
15 measurements.
- 16 • Preserves the dynamic of the inner control levels since it acts directly on the
17 voltage control signal.
- 18 • Robust against system parameters uncertainties and frequency variation, which
19 is of importance when considering scalable MGs.

20 This paper is organized as follows; In Section II, the modeling of islanded MGs is
21 described. Section III describes the main control levels of the proposed control strategy
22 and active resonance damping method. The performances of the proposed active
23 resonance damping method are analyzed in Section IV, while the system stability is
24 assessed in Section V. Experimental test results and discussions are presented in Section
25 VI. Finally, Section VII underlines the main contributions of this work.

II. SYSTEM DESCRIPTION AND MODELING

A. System description

A typical low voltage MG configuration is shown in Fig.1. It is mainly composed of multiple DG units with distributed energy resources and loads. Each DG unit consists of a locally controlled inverter with an output LC - L filters. The LC - L filter is employed to filter out switching harmonics and connect the DG inverter to the load bus.

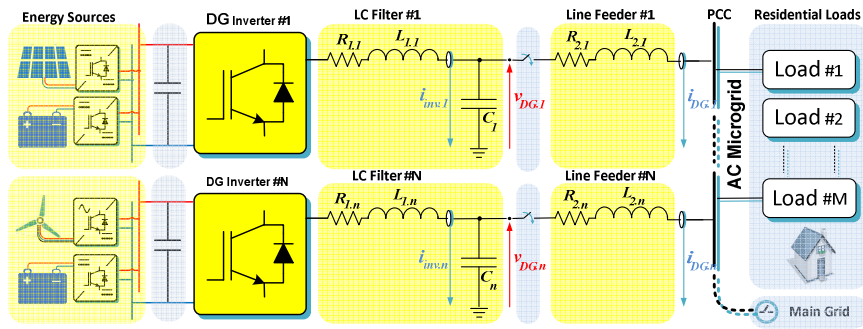


Fig. 1. Typical microgrid configuration

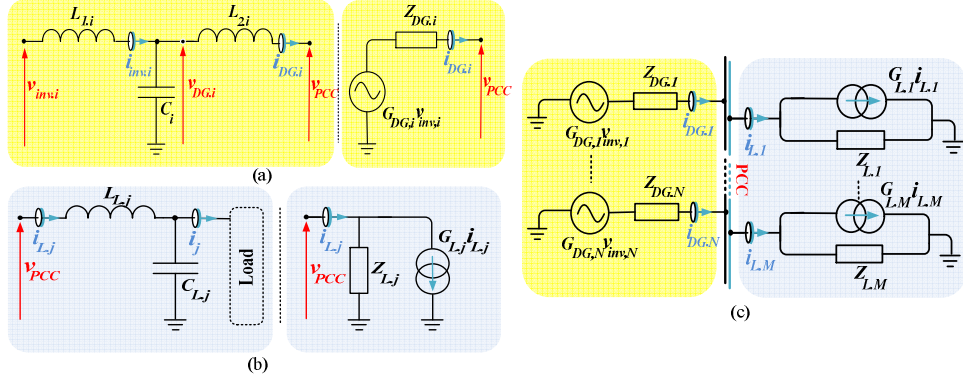
B. System modeling

Considering the coupling among the DG units and the background system, the development of a generalized model of MGs is necessary to analyze the main resonance characteristics and instability issues in MGs.

Firstly, given that the switching frequency is sufficiently high, each DG unit is modeled based on the dynamic behavior of its corresponding output LC - L filter as follows:

$$v_{PCC} = \frac{1}{L_{1,i}C_i s^2 + 1} v_{inv,i} - \frac{L_{1,i}s + L_{2,i}s(C_i s^2 + 1)}{L_{1,i}C_i s^2 + 1} i_{DG,i} \quad (1)$$

where, $v_{inv,i}$ and v_{PCC} represent the inverter voltage and the PCC voltage, respectively, while $i_{DG,i}$ represents the output current. $L_{1,i}$ and $L_{2,i}$ denote the inverter-side and the line-side filter inductances, respectively, while C_i represents the filter capacitance.



1

2 Fig. 2. Equivalent representations: Distributed generators (a), Loads (b), Microgrid (c).

3 Equation (1) corresponds to two Thévenin terminals consisting of an equivalent
 4 voltage source $G_{DG,i} v_{inv,i}$ and an output impedance $Z_{DG,i}$. The equivalent representation
 5 of DG units is illustrated in Fig.2 (a),

$$v_{PCC} = G_{DG,i} v_{inv,i} - Z_{DG,i} i_{DG,i} \quad (2)$$

6 Similarly, an equivalent load model is defined considering an LC filter interfaced load.

$$i_{L,j} = \frac{1}{L_{L,j} C_{L,j} s^2 + 1} i_j + \frac{C_{L,j} s}{L_{L,j} C_{L,j} s^2 + 1} v_{PCC} \quad (3)$$

7 where, $L_{L,j}$ and $C_{L,j}$ represent the load filter inductance and capacitance, respectively.

8 i_j and $i_{L,j}$ represent the load side and the load filter side current, respectively.

9 As illustrated in Fig. 2 (b), the load circuits can be represented with two Norton
 10 terminals consisting of an equivalent current source $G_{L,j} i_j$ and output admittance $Y_{L,j} =$
 11 $1/Z_{L,j}$.

$$i_{L,j} = G_{L,j} i_j + Y_{L,j} v_{PCC} \quad (4)$$

12 At this level, given the parallel representation shown in Fig.2 (c), and based on (2) and
 13 (4), the MG PCC's voltage can be expressed as follows [29]:

$$v_{PCC} = \frac{\sum_{i=1}^N G_{DG,i} Y_{DG,i} v_{inv,i} - \sum_{j=1}^M G_{L,j} i_j}{\sum_{i=1}^N Y_{DG,i} + \sum_{j=1}^M Y_{L,j}} \quad (5)$$

1 where, $Y_{DG,i} = 1/Z_{DG,i}$ represents the i^{th} DG unit admittance, while N and M represent
2 the number of DG units and loads, respectively.

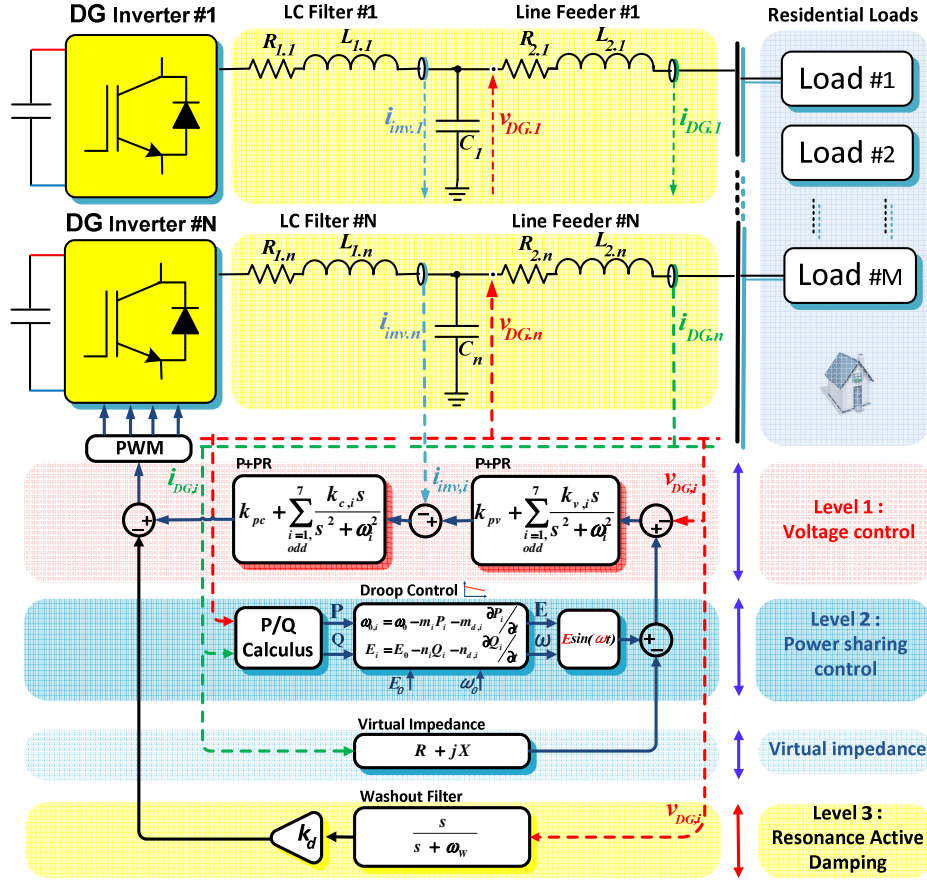
3 Equation (5) shows that the circuit configuration of MGs presents significant coupling
4 between the DG units and the background system. This situation increases the risk of
5 resonance interactions and propagation. For this aim, the development of advanced
6 active resonance damping methods is important to preserve MGs power quality and
7 stability.

8 III. PROPOSED ACTIVE DAMPING METHOD

9 As shown in Fig.3, the proposed control strategy adopts a hierarchical control
10 structure with multi-levels multi-loops control. The first and second control levels
11 include respectively a cascaded voltage-current controller and a communication-less
12 power sharing controller. The third control level is proposed to mitigate resonance
13 phenomena and preserve the stability of islanded MGs.

14 A. Level 1 : Voltage and Current control

15 The output voltage $v_{DG,i}$ of each DG unit is controlled via the control of the filter line
16 current $i_{inv,i}$.



1

2

Fig.3. Proposed hierarchical control strategy with resonance active damping

3

4

5

6

7

More specifically, a cascaded voltage and current controllers with selective harmonics compensation is designed using multi-resonant controllers. The use of resonant control offers the possibility to achieve selective harmonics compensation, which is important to enhance system disturbances rejection capabilities. The voltage and current control expressions are given as follows:

$$G_{c,i}(s) = k_{pc,i} + k_{c,i} \sum_{h=1,odd}^7 \frac{s}{s^2 + (\omega_0 h)^2} \quad (6)$$

$$G_{v,i}(s) = k_{pv,i} + k_{v,i} \sum_{h=1,odd}^7 \frac{s}{s^2 + (\omega_0 h)^2} \quad (7)$$

8

where $k_{pc,i}$ and $k_{pv,i}$, k_c and k_v represent, respectively, the proportional and resonant

9

gains of the inner and the outer loop controllers; and ω_0 is the angular frequency.

1 Note that, the use of an inner current control loop contributes to resonances
 2 attenuation. However, to achieve the desired attenuation, the proportional gain $k_{pc,i}$
 3 needs to be increased too much. This in fact enhances the control dynamic and improves
 4 disturbances rejection, but can cause resonance interaction between DG units.

5 *B. Level 2 : Power sharing control*

6 The interconnection of multiple DG units can lead to large circulating currents due
 7 essentially to the unbalanced system configuration between DG units, line impedance
 8 mismatches and so on. The presence of these currents will increase power losses and
 9 damage MG components. Therefore, the control of the power participation of each DG
 10 unit is required to achieve accurate power sharing and avoid circulating currents.

11 *B.1 Droop control loop*

12 The second control level includes a well-established power sharing method based on
 13 droop control [30]. Assuming that the DG unit output impedance is predominantly
 14 inductive, the following droop control expressions are used to control the participation of
 15 each DG unit.

$$\omega_{0,i} = \omega_0 - m_i P_i - m_{d,i} \frac{dP_i}{dt} \quad (8)$$

$$E_i = E_0 - n_i Q_i - n_{d,i} \frac{dQ_i}{dt} \quad (9)$$

16 Then, the voltage reference $v_{DG,i}^*$ is expressed as:

$$v_{DG,i}^* = E_i \sin (\omega_{0,i} t) \quad (10)$$

17 where, m_i , n_i , $m_{d,i}$ and $n_{d,i}$ represent the proportional and derivative droop slope
 18 coefficients. E_i and $\omega_{0,i}$ denote the dropped voltage amplitude and frequency.

19 These expressions include a proportional term that is synthesized to improve the power
 20 sharing accuracy, whereas the derivative term introduces a damping ratio that attenuates

1 transient, avoids large starting current oscillations and enhances the plug and play
 2 characteristic of the corresponding DG unit.

3 *B.2. Virtual impedance loop* In low voltage MGs, the output impedance of DG units
 4 presents a complex behavior with low X/R ratio. This situation may strengthen the
 5 coupling between the active and reactive power and entail the efficacy of the droop
 6 controller, expressed in (8) and (9). For this aim, a virtual impedance loop is added in
 7 order to enhance the inductive predominance of the output impedance. The virtual
 8 impedance is enforced by dropping the i^{th} DG voltage reference proportionally to the
 9 output current and its derivative.

$$v_{DG,i}^* = E_i \sin(\omega_{0,i} t) - Z_{D,i} i_{DG,i} \quad (11)$$

10 where, $Z_{D,i} = R_{D,i} + L_{D,i} s$, represents the i^{th} virtual impedance, with $R_{D,i}$ and $L_{D,i}$ the
 11 virtual resistance and inductance, respectively.

12 *C. Level 3 : Proposed Active Damping method*

13 The circuit configuration of islanded MGs is prone to experience severe resonance
 14 phenomena. These phenomena result in harmonics amplification, which affects power
 15 quality and increases the risk of instability. Moreover, the amplification of harmonic
 16 disturbances reduces the efficiency and reliability of MGs since it results in the increase
 17 of power losses and damages MG components. Thus, and as shown in Fig. 3, a third
 18 control level is added to the conventional DG control scheme in order to mitigate
 19 resonance harmonics amplification and propagation. The proposed control level acts
 20 directly on the voltage control signal in order to compensate for the resulting harmonic
 21 disturbances and overcome issues related to resonance phenomena. The proposed
 22 resonance damping control law is given in (12).

$$v_{inv,i}^* = v_{inv,i} - k_d \left(\frac{s}{s + \omega_w} \right) v_{DG,i} \quad (12)$$

1 where $v_{inv,i}^*$ represents the resulting inverter control voltage, $v_{DG,i}$ is the output voltage,
 2 and ω_w is the washout filter cut-off frequency. The value of ω_w is non-critical as long as
 3 it is chosen sufficiently lower than the switching frequency. The term k_d is the damping
 4 coefficient that can be used to scale up the damping ratio (see, Section V).

5 From equation (12), it can be seen that the voltage control signal is dropped
 6 proportionally to the undesired voltage harmonic disturbances. This introduces a resistive
 7 behavior around the resonance frequencies, which allows dampening the undesired
 8 resonance amplification. A Washout filter with inherent stability and unity gain
 9 characteristics is used to reconstruct the undesired resonance harmonic disturbances [31].
 10 The washout filter serves as a high pass filter that passes unchanged the undesired high
 11 frequency harmonic components and blocks out low frequency components.

12 Considering the context of MGs, this method presents the following advantages:

- 13 • **Dynamic**: Preserves the dynamic of the inner controllers as it acts on the control
 14 signal.
- 15 • **Robustness**: Does not require prior knowledge of system parameters and frequencies.
- 16 • **Simplicity**: Simple to design and implement using only the output voltage measure.

17 IV. RESONANCE DAMPING PERFORMANCES

18 A. Resonance damping model

19 In order to evaluate the efficacy of the proposed damping method, the expression given
 20 in (2) and (5) are rearranged to integrate the proposed method. The damping model of
 21 DG units is obtained by substituting (12) in (2) given that $v_{DG,i} = v_{PCC} + Z_{L2,i}i_{DG,i}$ as
 22 follows:

$$v_{PCC} = \frac{G_{DG,i}}{1 + k_d G_{DG,i} W(s)} v_{inv,i} - \frac{Z_{DG,i} + k_d G_{DG,i} W(s) Z_{L2,i}}{1 + k_d G_{DG,i} W(s)} i_{DG,i} \quad (13)$$

1 where, $W(s) = s/(s + \omega_w)$ represents the Washout filter transfer function.

2 The obtained expression can be expressed as:

$$v_{PCC} = G_{DG,i}^d v_{inv,i} - Z_{DG,i}^d i_{DG,i} \quad (14)$$

3 where, $G_{DG,i}^d$ and $Z_{DG,i}^d$ represent, the damped voltage gain and output impedance
4 expressions of the i^{th} DG unit, respectively.

5 Similarly, the damping model of islanded MGs considering multiple DG units and
6 loads is obtained by substituting (12) in (5) as follows:

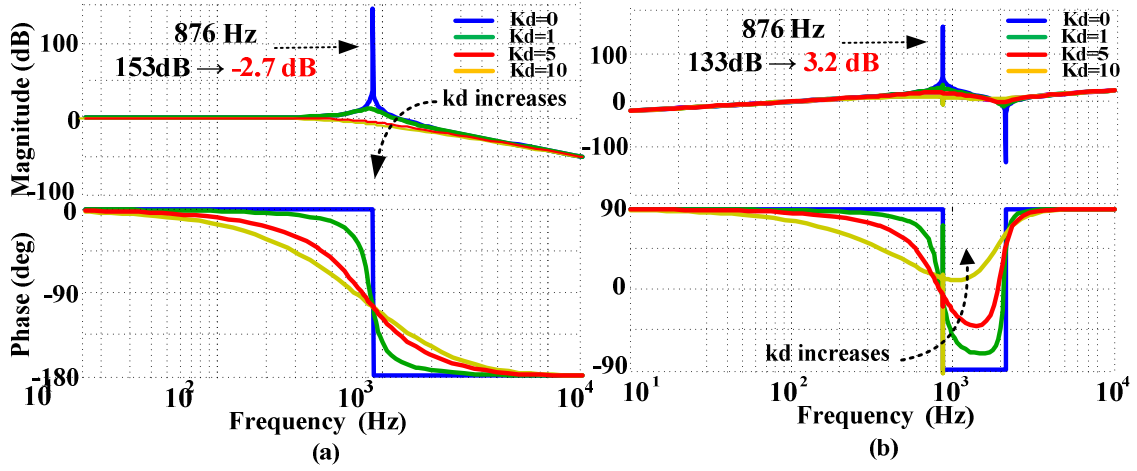
$$v_{PCC} = \frac{\sum_{i=1}^N G_{DG,i}^d Y_{DG,i} v_{inv,i} - \sum_{j=1}^M G_{L,j} i_j}{\sum_{i=1}^N Y_{DG,i}^d + \sum_{j=1}^M Y_{L,j}} \quad (15)$$

7 where $Y_{DG,i}^d = 1/Z_{DG,i}^d$ represents the damped i^{th} DG unit admittance.

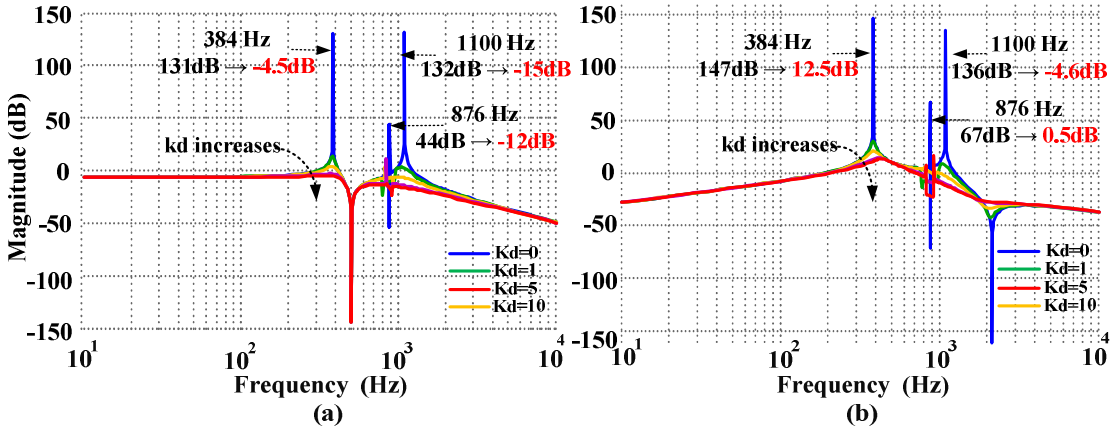
8 *B. Resonance damping evaluation*

9 The effectiveness of the proposed resonance damping method is evaluated based on the
10 frequency response of a single DG unit and a MG with multiple DG units and loads. The
11 obtained diagrams are illustrated in Figs. 6-7 using the parameters listed in the Appendix.

12 As illustrated in Fig. 6.a, the frequency response of a single DG unit highlights the
13 performances of the proposed damping for increasing values of the damping
14 coefficient k_d . This figure shows the presence of a single resonance peak with 153 dB at
15 876 Hz that is significantly reduced with the introduction of the proposed method to less
16 than 0 dB. The proposed method shows satisfactory damping performances alleviating
17 the resonance peak introduced by the $LC-L$ filter without affecting its harmonics
18 attenuation performances. The DG unit output impedance shown in Fig. 6.b tends to
19 have a resistive behavior around the resonance peak, which improves resonance
20 harmonics attenuation.



1
2 Fig. 6. Bode diagram: (a) voltage gain and (b) output impedance of as single distributed
3 generator before (blue) and after damping for $k_d \in [1 \ 10]$.



4
5 Fig. 7. Bode diagram of the DG side transfer functions ($v_{pcc}/v_{inv,i}$) (a) and the load
6 side transfer function (v_{pcc}/i_j) (b) before (blue) and after damping for $0 \leq k_d \leq 10$.

7 Similarly, the effectiveness of the proposed method is verified when considering a
8 typical MG configuration with two DG units and a common load. The obtained bode
9 diagrams are illustrated in Figs. 7. It can be seen that the MG is subject to two main
10 resonance peaks with up to 130 dB of magnitude at 384 Hz and 1100 Hz, and a
11 resonance peak due to the load circuit of 44 dB at 876 Hz. The introduction of the
12 proposed damping method allows reducing the resonances peaks to less than 0 dB. This
13 damping method shows strong resonance mitigation performances even in presence of
14 multiple resonances.

V. STABILITY ANALYSIS AND PARAMETERS SETTING

This section presents a general stability analysis in order to assess the effectiveness of the proposed damping method and its capability for attenuating resonance amplifications considering different values of k_d and ω_w . This is done by examining how the roots change with the variation of the damping coefficient k_d and the washout filter frequency ω_w . For the sake of simplicity, only the current and voltage proportional control gains are considered since the resonant gains do not affect the system dynamics, whereas the dynamic of the droop controller is much slower than that of the inner control loops. The closed-loop dynamics is derived by substituting the following control law into (2).

$$v_{inv,i} = \left((v_{DG,i}^* - v_{DG,i}) C_v(s) - i_{inv,i} \right) C_c(s) \quad (16)$$

being $i_{inv,i} = i_{DG,i} + v_{DG,i}/Z_{c,i}$ the filter inductor current, and the filter capacitor voltage $v_{DG,i} = Z_{L_{2,i}} i_{DG,i} + v_{PCC}$; $Z_{c,i} = 1/(C_i s)$ and $Z_{L_{2,i}} = L_{2,i} s$

The closed loop transfer function is given as follows:

$$v_{PCC} = \frac{G_{DG,i} C_{c,i} C_{v,i}}{1 + G_{DG,i} C_{c,i} (C_{v,i} Z_{c,i} + 1) / Z_{c,i}} v_{DG,i}^* - \frac{Z_{DG,i} + G_{DG,i} C_{c,i} ((C_{v,i} Z_{c,i} + 1) Z_{L_{2,i}} + Z_{c,i}) / Z_{c,i}}{1 + G_{DG,i} C_{c,i} (C_{v,i} Z_{c,i} + 1) / Z_{c,i}} i_{DG,i} \quad (17)$$

The obtained equation can be simplified to:

$$v_{PCC} = G_{CP,i} v_{DG,i}^* - Z_{CP,i} i_{DG,i} \quad (18)$$

where,, $G_{CP,i}$ and $Z_{CP,i}$ represent the closed loop voltage gain and output impedance.

Considering the damping method, the closed loop transfer function becomes:

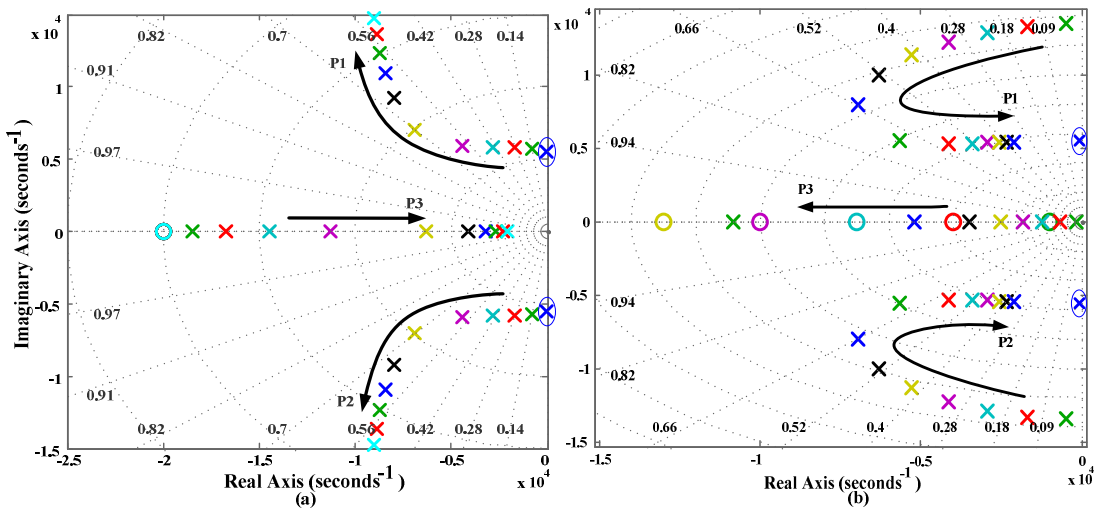
$$v_{PCC} = \frac{G_{DG,i}^d C_{c,i} C_{v,i}}{1 + G_{DG,i}^d C_{c,i} (C_{v,i} Z_{c,i} + 1) / Z_{c,i}} v_{DG,i}^* - \frac{Z_{DG,i}^d + G_{DG,i} C_{c,i} ((C_{v,i} Z_{c,i} + 1) Z_{L2,i} + Z_{c,i}) / Z_{c,i}}{1 + G_{DG,i}^d C_{c,i} (C_{v,i} Z_{c,i} + 1) / Z_{c,i}} i_{DG,i} \quad (19)$$

1 This equation can be simplified as:

$$v_{PCC} = G_{CP,i}^d v_{DG,i}^* - Z_{CP,i}^d i_{DG,i} \quad (20)$$

2 being $G_{CP,i}^d$ and $Z_{CP,i}^d$, the damped closed loop voltage gain and output impedance.

3 Based on (20), the system stability is evaluated using root locus diagrams. Fig. 8 shows
4 the root locus diagram for increasing values of k_d and ω_w . It can be seen, that the
5 system is initially marginally stable with an oscillatory behavior since it presents a pair
6 of complex conjugate poles (P1 and P2) near at the imaginary axis. These poles are
7 lightly dampened, which makes the system response prone to resonances oscillations. As
8 it can be observed from Fig. 8. (a), the introduction of the proposed method moves the
9 poles P1 and P2 toward the stable region. By increasing the coefficient k_d , the real part
10 of these poles increases and the damping ratio is improved, which results in a more
11 dampened system. P1 and P2 moves to higher frequencies when k_d is up to 5, which
12 facilitates their dampening.



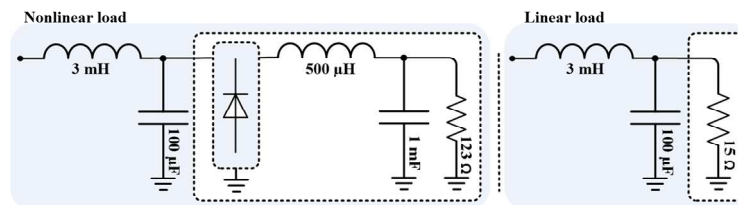
1 Fig. 8. Root-locus diagram without (encircled) and with damping for $0 \leq k_d \leq 10$ when
 2 $\omega_w = 5k \text{ rad.s}^{-1}$ (a), and for $1k \leq \omega_w \leq 20k \text{ rad.s}^{-1}$ when $k_d = 1$ (b).

3 Similarly, Fig. 8. (b) shows that by increasing the washout filter frequency, the poles
 4 P1 and P2 are attracted to the real axis making the system more dampened. However,
 5 when the washout filter frequency increases beyond the switching frequency, the poles
 6 P1 and P2 move toward the imaginary axis making the system less damped and more
 7 oscillatory. Moreover, the proposed damping method guarantees stable performances as
 8 it is based on a washout filter with inherent stability characteristics. This filter introduces
 9 a stable pole P3 that moves toward the stable region as the washout frequency increases

10 The parameters of the proposed damping method can be adjusted flexibly to improve
 11 the system stability and achieve the desired damping performances.

12 VI. EXPERIMENTAL TESTS

13 An experimental lab-scale islanded MG with two parallel DG units was built in the
 14 IREENA Laboratory in order to verify the effectiveness of the proposed resonance active
 15 damping control strategy. The experimental test bench comprises two SEMIKRON
 16 inverters with similar LC-L output filters supplying linear and rectifier type nonlinear
 17 loads. The proposed hierarchical control strategy is implemented on a dSPACE Micro
 18 Auto Box control prototyping system. The implementation of the control requires 39.2
 19 μs whereas the proposed damping method requires $2.1 \mu\text{s}$, based on $100 \mu\text{s}$ sampling.



20
 21 Fig. 9. Loads circuit representation

22 A. Case 1 – Linear load

1 The efficacy of the proposed hierarchical control strategy is evaluated when both DG

2 units are supplying a common linear load. The load circuit is shown in Fig. 9. The

3 measured voltage and current waveforms are shown in Fig. 10 before and after damping.

4 The comparison between the DG#1, DG#2 and the PCC voltage and current waveforms

5 shows similar resonance characteristics with high frequency harmonic distortions.

6 Moreover, and as it can be appreciated from the harmonic spectrum illustrated in Fig. 12

7 (a), the whole MG is affected by at least three resonance peaks around 1020 Hz. This

8 situation indicates that the resonance harmonic disturbances may propagate and affect

9 the whole MG performances even when introduced by a single part. It is shown that the

10 introduction of the proposed active damping method allows alleviating the undesired

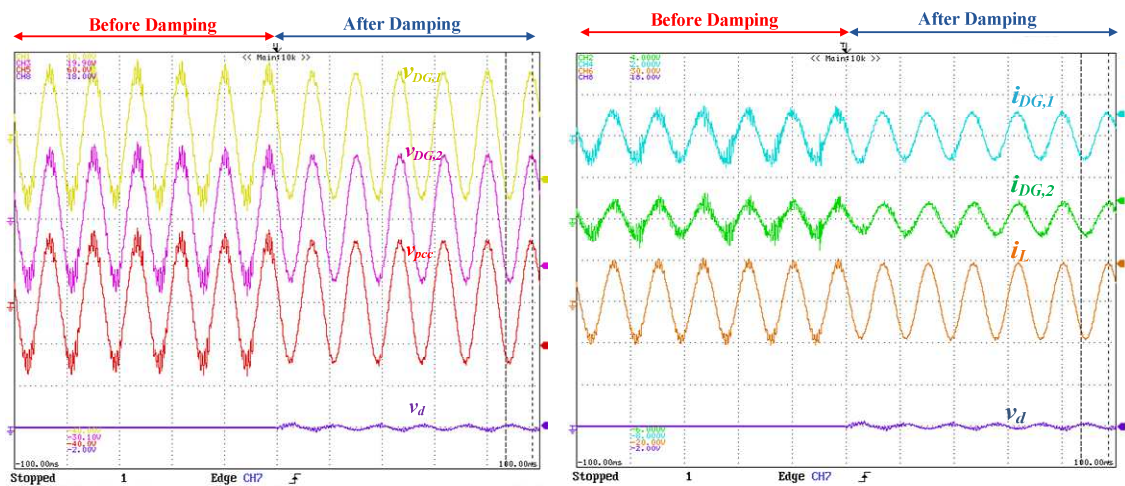
11 resonance harmonics. As reported in Table I, the introduction of the proposed damping

12 method reduces noticeably the amplitude of the resonance harmonics that varies from

13 4.97 V and 12.7 V before damping, to 0.17 V and 2.12V after damping. The output

14 voltage quality is considerably enhanced by reducing the total harmonic distortion

15 content from 6.6% before damping to 1.1% after damping.



16

17 Fig. 10. Measured DG #1, DG #2 and PCC voltage (left) and current (right) waveforms,

18 and the damping signal before and after damping – Case 1 : Linear load[x-axis:

19 20ms/div; y-axis: 10A/div - 100V/div].

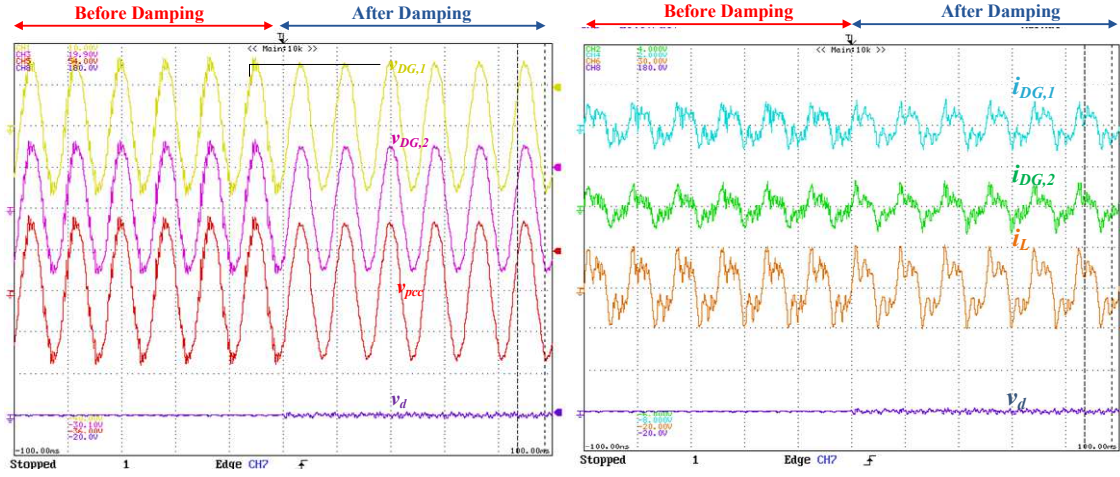


Fig. 111. Measured DG #1, DG #2 and PCC voltage (left) and current (right) waveforms, and the damping signal before and after damping – Case 2 : Nonlinear load[x-axis: 20ms/div; y-axis: 10A/div - 100V/div].

TABLE I: RESONANCES DAMPING PERFORMANCES

Frequency	Linear load		Nonlinear load	
	Before	After	Before	After
900 Hz	4.97 V	2.12 V	-	-
1020 Hz	12.7 V	1.77 V	5.81 V	1.48 V
1140 Hz	5.47 V	0.17 V	12.5 V	0.99 V
1260 Hz	-	-	4.83 V	1.44 V

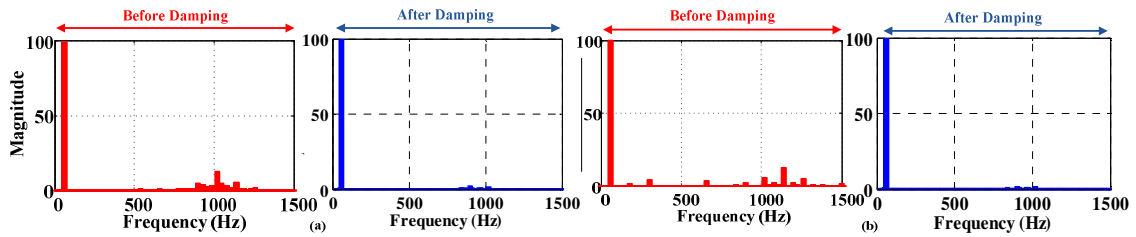


Fig.12. PCC's voltage harmonic spectrum before and after damping – Case 1 : Linear load (a), Case 2 : Nonlinear load (b).

B. Case 2 – Nonlinear load

The efficacy of the proposed control strategy is evaluated when the nonlinear load shown in Fig. 9 is supplied. This highly nonlinear load stands for a widespread of load applications in MGs. The measured DG#1, DG#2 and load voltage and current

1 waveforms are shown in Fig. 11 before and after damping. High frequency voltage and
2 current oscillations are noticed due mainly to resonances excitation. As shown in the
3 harmonic spectrum illustrated in Fig. 12 (b), these resonances oscillations appear at high
4 frequencies around 1140Hz. The introduction of the proposed active damping method
5 allows mitigating the undesired harmonic disturbances and considerably reduces the
6 amplitude of the resonance harmonics that varies from 4.83 to 12.5 V before damping,
7 and from 0.99 V to 1.48 V after damping. Moreover, this dampening method allows
8 enhancing the voltage waveform quality by eliminating the undesired lower frequency
9 harmonics that introduces the supplied nonlinear load at 300 Hz and 660 Hz. The output
10 voltage quality is considerably enhanced by reducing the total harmonic distortion
11 content to 1.9 %, while it was 6.9 % before damping.

12 It is worth mentioning, that the proposed active resonance damping control level
13 achieves suitable damping performances attenuating the undesired resonance
14 amplifications without affecting the performances of the inner control levels.

15 VII. CONCLUSIONS

16 An advanced hierarchical control strategy with active resonance damping was
17 designed to control DG based MGs operations and dampen out the undesired resonance
18 amplifications. This control strategy comprises three control levels including voltage
19 and current control, power sharing control, and active resonance damping control. The
20 proposed active resonance damping control uses a filter based approach to reconstruct
21 and compensate for the undesired resonances harmonics. The use of a Washout filter
22 with inherent stability characteristics has been proposed to extract the undesired
23 resonances harmonics content. The effectiveness of the proposed active damping method
24 has been verified and its stability investigated using a comprehensive numerical analysis
25 considering variable damping coefficient values. The experimental tests have shown that

1 the proposed control strategy demonstrates effective performances for resonances
2 damping, compensating for multiple resonances without affecting the system dynamic.

3 ACKNOWLEDGEMENT

4 This work was supported by FEDER and RFI Electronique WISE.

5 APPENDIX

6 Power stage parameters: $E_0 = \sqrt{2} \times 110\text{V}$, $\omega_0 = 2\pi 60 \text{ rad.s}^{-1}$, $V_{dc} = 250 \text{ V}$, $F_s = 10 \text{ kHz}$,
7 $L_{1,i} = 1 \text{ mH}$, $L_{2,i} = 0.2 \text{ mH}$, $C_i = 33 \text{ }\mu\text{F}$.

8 Control parameters: Level 1 : $k_{pc} = 5.21$, $k_c = 60$, $k_{pv} = 2.58$, $k_v = 70$. Level 2: $m_i = 0.003$
9 $\text{rad.s}^{-1} \cdot \text{W}^{-1}$, $n_i = 0.005 \text{ V} \cdot \text{Var}^{-1}$, $m_{d,i} = 0.00004 \text{ rad} \cdot \text{W}^{-1}$, $n_{d,i} = 0.00003 \text{ V} \cdot \text{s} \cdot \text{VAr}^{-1}$,
10 $L_{d,i} = 500 \text{ }\mu\text{H}$. Level 3 : $k_d = 1$, $\omega_w = 2\pi 1000 \text{ rad} \cdot \text{s}^{-1}$.

11 REFERENCES

- 12 [1]A. Gupta, S. Doolla, and K. Chatterjee, "Hybrid AC-DC Microgrid: Systematic
13 Evaluation of Control Strategies," *IEEE Trans. Smart Grid*, vol. 9, no. 4, pp.
14 3830–3843, Jul. 2018.
- 15 [2]S. Kumar Tiwari, B. Singh, and P. K. Goel, "Design and Control of Microgrid Fed by
16 Renewable Energy Generating Sources," *IEEE Trans. Ind. Appl.*, vol. 54, no. 3,
17 pp. 2041–2050, May 2018.
- 18 [3]M. Nasir, H. A. Khan, A. Hussain, L. Mateen, and N. A. Zaffar, "Solar PV-based
19 scalable DC microgrid for rural electrification in developing regions," *IEEE*
20 *Trans. Sustain. Energy*, vol. 9, no. 1, pp. 390–399, Jan. 2018.
- 21 [4]M. Meral, and D. Çelik, "A comprehensive survey on control strategies of distributed
22 generation power systems under normal and abnormal conditions," *Annual*
23 *Reviews in Control*, 47, pp. 112-132, 2019.

- 1 [5]D. Çelik, and M. Meral, “A novel control strategy for grid connected distributed
2 generation system to maximize power delivery capability,” *Energy*, vol. 186, p.
3 115850, 2019.
- 4 [6]M. Hajiakbari Fini and M. E. Hamedani Golshan, “Determining optimal virtual inertia
5 and frequency control parameters to preserve the frequency stability in islanded
6 microgrids with high penetration of renewables,” *Electr. Power Syst. Res.*, vol.
7 154, pp. 13–22, Jan. 2018.
- 8 [7]Y. S. Kim, E. S. Kim, and S. Il Moon, “Frequency and voltage control strategy of
9 standalone microgrids with high penetration of intermittent renewable generation
10 systems,” *IEEE Trans. Power Syst.*, vol. 31, no. 1, pp. 718–728, 2016.
- 11 [8]J. He, X. Liu, M. Lei, and C. Wang, “A Broad Frequency Range Harmonic Reduction
12 for Cascaded Power Cells Based Islanded Microgrid with Lumped PCC Filter,”
13 *IEEE Trans. Power Electron.*, pp. 1–1, Jan. 2020.
- 14 [9]D. Sharma and S. Mishra, “Disturbance-Observer-Based Frequency Regulation
15 Scheme for Low-Inertia Microgrid Systems,” *IEEE Syst. J.*, vol. 14, no. 1, pp.
16 782–792, Mar. 2020.
- 17 [10] A. Akhavan, H. R. Mohammadi, and J. M. Guerrero, “A comprehensive control
18 system for multi-parallel grid-connected inverters with LCL filter in weak grid
19 condition,” *Electr. Power Syst. Res.*, vol. 163, pp. 288–300, Oct. 2018.
- 20 [11] F. Wu, J. Ye, X. Luo, Z. Zhang, and Y. Li, “Resonance characteristic analysis and
21 damping control for LCL-filter-based voltage source converter during bus
22 transfer,” *Electr. Power Syst. Res.*, vol. 150, pp. 144–151, Sep. 2017.
- 23 [12] N. Rashidirad, M. Hamzeh, K. Sheshyekani, and E. Afjei, “High-Frequency
24 Oscillations and Their Leading Causes in DC Microgrids,” *IEEE Trans. Energy
25 Convers.*, vol. 32, no. 4, pp. 1479–1491, Dec. 2017.

- 1 [13] A. Akhavan, H. R. Mohammadi, J. C. Vasquez, and J. M. Guerrero, "Coupling
2 effect analysis and control for grid-connected multi-microgrid clusters," *IET
3 Power Electron.*, vol. 13, no. 5, pp. 1059–1070, Apr. 2020.
- 4 [14] F. Yazdi and S. H. Hosseinian, "Variable cost model predictive control strategies
5 for providing high-quality power to AC microgrids," *IET Gener. Transm. Distrib.*,
6 vol. 13, no. 16, pp. 3623–3633, Aug. 2019.
- 7 [15] Q. Ye, R. Mo, and H. Li, "Multiple resonances mitigation of paralleled inverters
8 in a solid-state transformer (SST) Enabled AC Microgrid," *IEEE Trans. Smart
9 Grid*, vol. 9, no. 5, pp. 4744–4754, Sep. 2018.
- 10 [16] M. Lu, X. Wang, P. C. Loh, and F. Blaabjerg, "Resonance Interaction of
11 Multiparallel Grid-Connected Inverters With LCL Filter," *IEEE Trans. Power
12 Electron.*, vol. 32, no. 2, pp. 894–899, Feb. 2017.
- 13 [17] A. Luo, Q. Xu, F. Ma, and Y. Chen, "Overview of power quality analysis and
14 control technology for the smart grid," *J. Mod. Power Syst. Clean Energy*, vol. 4,
15 no. 1, pp. 1–9, Jan. 2016.
- 16 [18] Y. Han *et al.*, "Modeling and Stability Analysis of LCL-Type Grid-Connected
17 Inverters: A Comprehensive Overview," *IEEE Access*, vol. 7, pp. 114975–
18 115001, Aug. 2019.
- 19 [19] M. Routimo and H. Tuusa, "LCL type supply filter for active power filter -
20 Comparison of an active and a passive method for resonance damping," in *PESC
21 Record - IEEE Annual Power Electronics Specialists Conference*, 2007, pp. 2939–
22 2945.
- 23 [20] A. K. Balasubramanian and V. John, "Analysis and design of split-capacitor
24 resistiveinductive passive damping for LCL filters in grid-connected inverters,"
25 *IET Power Electron.*, vol. 6, no. 9, pp. 1822–1832, 2013.

- 1 [21] Y. Tang, W. Yao, P. C. Loh, and F. Blaabjerg, "Design of LCL Filters with LCL
2 Resonance Frequencies beyond the Nyquist Frequency for Grid-Connected
3 Converters," *IEEE J. Emerg. Sel. Top. Power Electron.*, vol. 4, no. 1, pp. 3–14,
4 Mar. 2016.
- 5 [22] M. A. Awal, H. Yu, L. Della Flora, W. Yu, S. Lukic, and I. Husain, "Observer
6 based admittance shaping for resonance damping in voltage source converters
7 with LCL filter," in *2019 IEEE Energy Conversion Congress and Exposition,
8 ECCE 2019*, 2019, pp. 4455–4462.
- 9 [23] J. Dannehl, F. W. Fuchs, S. Hansen, and P. B. Thøgersen, "Investigation of active
10 damping approaches for PI-based current control of grid-connected pulse width
11 modulation converters with LCL filters," *IEEE Trans. Ind. Appl.*, vol. 46, no. 4,
12 pp. 1509–1517, Jul. 2010.
- 13 [24] Y. Guo, L. Chen, X. Lu, J. Wang, T. Zheng, and S. Mei, "Region-Based Stability
14 Analysis for Active Dampers in AC Microgrids," *IEEE Trans. Ind. Appl.*, vol. 55,
15 no. 6, pp. 7671–7682, Nov. 2019.
- 16 [25] D. J. L. M. F. F., "Filter-Based Active Damping of Voltage Source Converters
17 With LCL Filter," *IEEE Trans. Ind. Electron.*, vol. 58, no. 8, pp. 3623–3633,
18 2011.
- 19 [26] W. Yao, Y. Yang, X. Zhang, F. Blaabjerg, and P. C. Loh, "Design and Analysis of
20 Robust Active Damping for LCL Filters Using Digital Notch Filters," *IEEE
21 Trans. Power Electron.*, vol. 32, no. 3, pp. 2360–2375, Mar. 2017.
- 22 [27] J. Yuan, A. Al Durra, and E. El-Sadaany, "Adaptive digital notch filter based on
23 online grid impedance estimation for grid-tied LCL filter systems," *Electr. Power
24 Syst. Res.*, vol. 172, pp. 183–192, Jul. 2019.
- 25 [28] A. Saim, A. Houari, J. M. Guerrero, A. Djerioui, M. Machmoum, and M. A.

1 Ahmed, "Stability analysis and robust damping of multiresonances in distributed-
2 generation-based islanded microgrids," *IEEE Trans. Ind. Electron.*, vol. 66, no.
3 11, pp. 8958–8970, Nov. 2019.

4 [29] J. He, Y. W. Li, D. Bosnjak, and B. Harris, "Investigation and Active Damping of
5 Multiple Resonances in a Parallel-Inverter-Based Microgrid," *IEEE Trans. Power
6 Electron.*, vol. 28, no. 1, pp. 234–246, Jan. 2013.

7 [30] A. Saim, R. Mellah, A. Houari, M. Machmoum, and A. Djerioui, "Adaptive
8 resonant based multi-loop control strategy for parallel distributed generation units
9 in standalone microgrid application," *Electr. Power Syst. Res.*, vol. 143, 2017.

10 [31] J. H. Chow and R. J. Thomas, *Systems and control theory for power systems*.
11 1995.

12